0.23 ± 0.30 for the smaller wave. Average departure from the great circle path was 1.8 ± 4.1° for the larger wave and −2.2 ± 9.4° for the smaller.
11. Because amplitudes carry information about the wavefield interference, at each frequency, we modeled the real and imaginary components for each record, rather than just the phase. Amplitudes are corrected for geometrical spreading on a uniform sphere, instrument-site response, and attenuation. In our tomographic inversions, we solved simultaneously for the velocity parameters and the six wavefield parameters per event. In an inversion that attempts to match all the amplitudes from all events simultaneously, we found the best attenuation factor for the region as a whole and the best, single amplitude correction factor for each station. At 25 s, the attenuation quality factor Q is ≥ 125.
12. In a nonlinear inversion, the results may depend on model assumptions. We ran more than 80 different inversions with different starting models, grids, and approaches to damping to understand which features of the models are robust. In the interior of the grid, we applied either a smoothness criterion so that the inversion will tend to find the smoothest set of changes to the starting model that satisfies the data or a damping criterion that tends to minimize the size of the changes to the starting model. In the inversions presented in Fig. 3, we used a 13 by 15 grid of velocity nodal points, spaced 1° apart from 11° to 20°S and extending 6° to the east and west of the ridge axis. Near the center of the grid and near the axis, points are spaced 0.5° apart. At each latitude, the grid points are shifted so that the center of the grid is at the ridge axis. The outer grid points are only lightly damped so that their values are free to vary to represent time delays that accumulate outside the area of interest.
13. The MELT Seismic Team, *Science* **280**, 1215 (1998).
14. D. S. Scheirer, D. W. Forsyth, M.-H. Cormier, K. C. Macdonald, *ibid.*, p. 1221.
15. C. J. Wolfe and S. C. Solomon, *ibid.*, p. 1230.
16. D. R. Toomey, W. S. D. Wilcock, S. C. Solomon, W. C. Hammond, J. A. Orcutt, *ibid.*, p. 1224.
17. M. A. Eberle and D. W. Forsyth, *Nature,* in press.
18. D. Zhao *et al.*, *Science* **278**, 254 (1997).
19. J. J. Mahoney *et al.*, *Earth Planet. Sci. Lett.* **121**, 173 (1994).
20. M. D. Kurz, J. J. Mahoney, J. M. Sinton, in preparation.
21. M.-H. Cormier, D. S. Scheirer, K. C. Macdonald, *Mar. Geophys. Res.* **18**, 53 (1996).
22. D. K. Blackman *et al.*, *Geophys. J. Int.* **127**, 415 (1996).
23. G. Hirth and D. L. Kohlstedt, *J. Geophys. Res.* **100**, 1981 (1995).
24. S. Karato and P. Wu, *Science* **260**, 771 (1993).
25. W. Friederich, E. Wielandt, S. Stange, *Geophys. J. Int.* **119**, 931 (1994).
26. P. Wessel and W. H. F. Smith, *Eos* **72**, 441 (1991).
27. This project is part of the Ridge Inter-Disciplinary Global Experiments program and is funded by the NSF. We thank D. Scheirer and S.-H. Hung for help in generating maps and handling data and C. Wolfe for a constructive review. The Generic Mappings Tools plotting program (*26*) was used in several figures.

18 February 1998; accepted 21 April 1998

The Radio-Frequency Single-Electron Transistor (RF-SET): A Fast and Ultrasensitive Electrometer

R. J. Schoelkopf,* P. Wahlgren, A. A. Kozhevnikov, P. Delsing, D. E. Prober

A new type of electrometer is described that uses a single-electron transistor (SET) and that allows large operating speeds and extremely high charge sensitivity. The SET readout was accomplished by measuring the damping of a 1.7-gigahertz resonant circuit in which the device is embedded, and in some ways is the electrostatic "dual" of the well-known radio-frequency superconducting quantum interference device. The device is more than two orders of magnitude faster than previous single-electron devices, with a constant gain from dc to greater than 100 megahertz. For a still-unoptimized device, a charge sensitivity of $1.2 \times 10^{-5}\ e/\sqrt{\text{hertz}}$ was obtained at a frequency of 1.1 megahertz, which is about an order of magnitude better than a typical, $1/f$-noise-limited SET, and corresponds to an energy sensitivity (in joules per hertz) of about 41 $\hbar$.

Methods for performing more-sensitive electrical measurements are often instrumental in enabling new physics and technology. Improvements in measurements can be accomplished either through refinement of traditional devices or by developing devices that rely on different physical principles. An example of the latter are superconducting quantum interference devices (SQUIDs), which use the phenomenon of flux quantization in a superconducting loop and are the most sensitive magnetometers (*1*) available. Besides magnetometry, SQUIDs have also been adapted to a wide range of applications where amplifiers are needed for low-level signals and low-impedance sources.

We report the development of an extremely sensitive electrometer, based on a new type of SET—the radio-frequency SET or RF-SET. First proposed by Averin and Likharev (*2*) and demonstrated by Fulton and Dolan (*3*), the SET is the electrostatic "dual" (*4*) of the SQUID and is able to measure a small fraction of an electron's charge. As such, single-electron devices are complementary to SQUIDs and should be the measurement technology of choice for sensitive, high-impedance applications. However, conventional SET-based electrometers have been limited by slow operation speeds, typically 1 kHz or less. Furthermore, the charge sensitivity at these low frequencies, while typically much higher than that of conventional electrometers, is limited by $1/f$ noise (*5*) due to the motion of background charges. The RF-SET, however, can operate even at frequencies in excess of 100 MHz, where the $1/f$ noise due to background charge motion is completely negligible. In fact, we describe how optimized versions of this device could allow electrometry at the quantum limit, with an energy sensitivity of a few $\hbar$ ($\hbar \equiv 1.054 \times 10^{-34}$ J/Hz).

With the advent of this truly high-speed and more sensitive electrometer, many of the proposed applications of single electronics, including an electron-counting current standard (*6*) and advanced photodetectors (*7*), become much more practical. For example, at the present performance levels, the RF-SET has the sensitivity and speed to count electrons at frequencies >10 MHz (that is, measure a current on the order of picoamperes, electron by electron) with very good signal-to-noise (S/N) ratio. New physics experiments can be envisioned in "single-charge dynamics," such as the direct observation of Bloch and single-electron tunneling oscillations (*2, 8*), and the monitoring of tranport processes at the single-charge level in a variety of systems.

Most Coulomb blockade (SET) electrometers use a double-junction structure with a central metallic island that is capacitively coupled to the input. Under the proper conditions, such a device has an onset of current that is controlled by the potential of the island. The onset is periodic in the gate charge, q_g, coupled onto the island via the gate capacitor, with a period equal to the charge of a single electron, e. The gate charge, q_g, can be continuously varied and is defined as $q_g = C_g V_g$, where C_g is the gate capacitance and V_g is the gate voltage. Usually, the SET is current-biased just above threshold, and the drain-to-source voltage is monitored with a high-impedance voltage amplifier at room temperature. Despite their limitations, such SET electrometers have already been used to observe macroscopic charge quantization (*9*), to characterize the performance of single-electron pumps and traps (*10, 11*), and to measure the local chemical potential variations (*12, 13*) of semiconducting systems.

In order to display a strong Coulomb blockade and the desired sharp onset of

R. J. Schoelkopf, A. A. Kozhevnikov, D. E. Prober, Departments of Applied Physics and Physics, Yale University, New Haven, CT 06520–8284, USA.
P. Wahlgren and P. Delsing, Department of Microelectronics and Nanoscience, Chalmers University of Technology and Göteborg University, S-412 96 Göteborg, Sweden.

*To whom correspondence should be addressed. E-mail: rob.schoelkopf@yale.edu

current, each junction of the SET must be of the order of the resistance quantum, $R_K = h/e^2 = 26$ kilohms, leading to a typical device resistance of $R = 100$ kilohms or more. Given the capacitive load for the cabling ($C_l = 0.1$ to 1 nF) to the room-temperature amplifier, the bandwidth is limited to $f < 1/2\pi RC_l$, or less than a few kilohertz. Note, however, that the intrinsic limit on the speed of the SET should be determined by the RC (resistance times capacitance) time constant of the tunnel junctions themselves (*14*), which can be greater than 10 GHz.

One approach (*15, 16*) for improving the speed of SET electrometers has used a cryogenic voltage amplifier, integrated in close proximity to the SET, to minimize the capacitive load. The total capacitance, although it includes the capacitance of the GaAs high electron mobility transistor (HEMT) used as the amplifier, can be less than 1 pF; this technique has allowed speeds (*15*) as high as 700 kHz. There are significant engineering challenges involved, however, including undesirable heating of the SET when the HEMT is optimally biased. The noise performance was also limited by the HEMT. Recently, very good noise performance (*17*) has been obtained at about 4 kHz, using a low-impedance, room-temperature current amplifier to measure the output of a voltage-biased SET. Although such a scheme avoids RC limits on the gain, the noise contribution of the postamplifier increases very rapidly with frequency above $1/2\pi RC_l$, and the noise bandwidth of the system is thus unlikely to exceed a few kilohertz.

In the RF-SET, the readout of the charge state of the device is accomplished by monitoring the damping of a high-frequency resonant circuit to which the SET is connected, rather than by measuring either the current or the voltage. This readout scheme offers many advantages. By using a low-impedance (50 ohm) high-frequency amplifier, the capacitance of the cabling between SET and the amplifier becomes unimportant (*18*). Once it is physically and thermally separated from the SET, the amplifier can be optimized without the constraint of very low power dissipation required for operation at millikelvin temperatures. Finally, because the readout is performed at a high frequency, there is no amplifier contribution to the $1/f$ noise.

A schematic of our measurement apparatus is shown in Fig. 1. The SET itself was a typical Al-based SET, fabricated using electron-beam lithography, a suspended resist bridge, and a double-angle evaporation technique (*19*). The source (S) of the SET was grounded, and the connection to the drain (D) was made by pressing a chip inductor, with an inductance of 27 nH, between a contact pad on the SET chip and the center pin of a 50-ohm semirigid coaxial cable. This cable connected the sample chip, held at 45 mK on the mixing chamber of a dilution refrigerator, to the main He bath, approximately 1 m away. The cable fed a 1.25 to 1.75 GHz HEMT-based low-noise amplifier, with an input impedance of 50 ohms.

The value of the series inductance was chosen so that it formed a resonant circuit with the parasitic capacitance, $C_{pad} \approx 0.33$ pF, of the contact pad to the SET, with a resonance frequency of 1.7 GHz. A monochromatic signal at this resonance frequency, which we will refer to as the "carrier," was launched toward the SET, and the power reflected was then amplified and rectified. For a small 1.7-GHz signal, the variation in the reflected carrier power as a function of the gate voltage is shown (Fig. 2B). The transistor's dc drain-source bias was zero except for a small audio frequency excitation, which was introduced via a bias-tee [(*20*); at 45 mK], and was used to monitor the dc drain-source conductance. The dc conductance displays the familiar Coulomb blockade oscillations, with sharp conductance peaks separated by uniform intervals in gate voltage, $\delta V_g = e/C_g$, corresponding to the addition of individual electrons to the transistor's island. It is apparent that the reflected carrier power is strongly correlated with the transistor's conductance. When the conductance is a minimum and the transistor is in its blockaded state, then the reflected power is high, as would be expected for a transmission line terminated with an open circuit. When the transistor becomes conducting, some fraction of the carrier is dissipated in the SET, and the reflected power decreases.

The relative change in the reflected carrier power is small, because even the minimum resistance of the transistor is large compared to the characteristic impedance of the microwave system. The inductor and capacitor serve at resonance to transform this impedance upward, and thereby increase the change in carrier reflection by a factor of about 40 (*21*). For best sensitivity, the RF-SET was held at zero drain-source dc bias, and an ac voltage amplitude approximately equal to the threshold voltage (*22*) was used. The dc conductance and

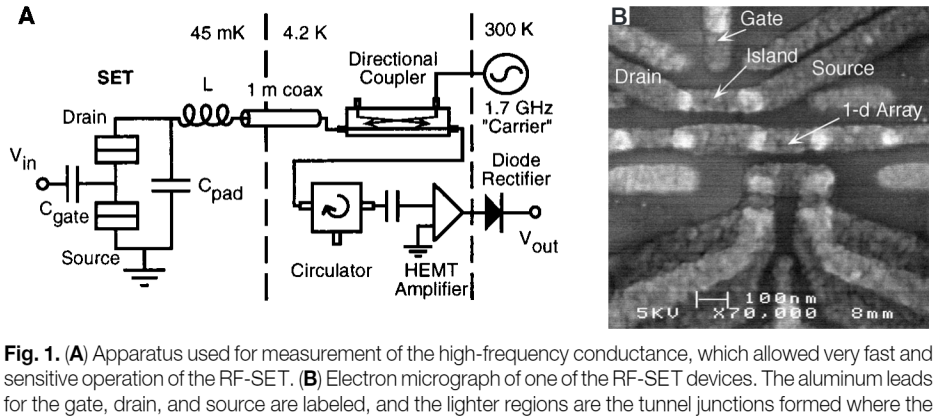

Fig. 1. (**A**) Apparatus used for measurement of the high-frequency conductance, which allowed very fast and sensitive operation of the RF-SET. (**B**) Electron micrograph of one of the RF-SET devices. The aluminum leads for the gate, drain, and source are labeled, and the lighter regions are the tunnel junctions formed where the drain and source overlap the island. The SET is fabricated in close proximity to a long (64 junction) one-dimensional array of similar junctions, to allow a search for single-electron tunneling oscillations.

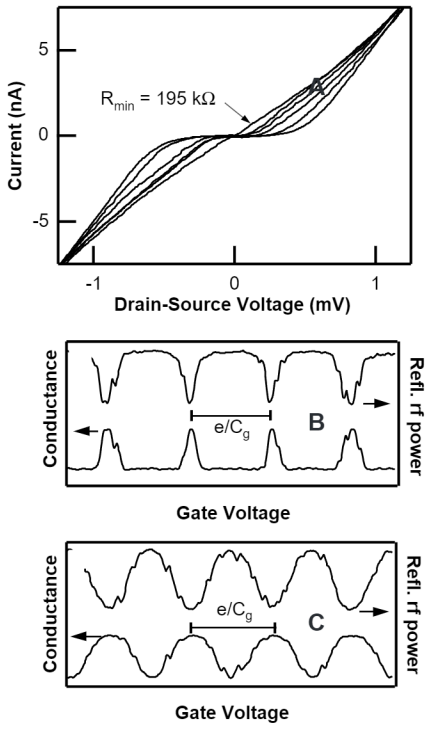

Fig. 2. (**A**) Current-voltage characteristics of SET as a function of gate voltage. (**B**) The small-signal dc conductance (lower trace) at zero drain-source bias for the SET, displaying the periodic conductance maxima when additional electrons are added to the island. The upper trace shows the total reflected power for a small RF signal at 1.7 GHz under the same conditions. (**C**) The dc conductance and ac reflected power for a large carrier power and zero dc bias, corresponding to the optimum operating conditions for the RF-SET.

reflected carrier power for these conditions are shown (Fig. 2C). The large ac amplitude smooths out the conductance oscillations into an approximately sinusoidal form by sampling a wider range of drain-source bias voltage, but the fractional variation of the reflection remains unchanged. Note that the transfer function for the reflected power versus gate charge (or gate voltage, $q_g = C_g V_g$) is similar to the curves of dc voltage versus gate charge for the usual type of SET when it is current-biased near threshold.

We refer to the device operation described above as an RF-SET, because there are some similarities with the well-known RF-SQUID (*1*). For example, both use the change in damping of a resonant tank circuit to read out the charge (or flux) state of the device. The RF-SET is probably most nearly related to the double SQUID (D-SQUID) (*23*), a relatively new variety of RF-SQUID with two junctions and two quantization loops. However, the operation of the RF-SET is not an exact analog to any common type of SQUID. Because space does not permit, a detailed examination of the duality to the RF-SQUID and a full discussion of the design and optimization of the RF-SET will be published later (*24*).

As mentioned above, we expect that the high-frequency measurement of the transistor's conductance will permit a sensitive and very fast readout of the charge coupled through the gate capacitor. Both the microwave amplifier and rectifying diode have bandwidths >100 MHz. The impedance of the SET should respond to changes of the gate on even faster time scales, with a bandwidth (*14*) of the order $1/2\pi R_J C_J \approx 10$ GHz. The rapid response of the RF-SET in the time domain can be seen by examining the amplified output of the rectifying diode on a digitizing oscilloscope. The average of 2048 individual traces, taken with a large amplitude ($\Delta q_g = C_g V_g \approx 5.5\ e$ peak-to-peak) 10-kHz triangle-wave signal applied to the gate, is shown (Fig. 3A). The output indeed follows the sinusoidal transfer function, passing through five successive maxima (one for each electron added to the island), and then reversing at the turning points of the gate signal (dotted line). The S/N ratio is also quite high.

The device can also be used as a linear amplifier for small signals with a charge less than $|e|$, when the gate is biased at a charge corresponding to the maximum slope of the sinusoidal response. The gate signal then causes an amplitude modulation on the carrier (*25*) at the signal frequency. At large gate frequencies, it is more convenient to use an RF spectrum analyzer to see this modulation in the output of the rectifying diode. Such a spectrum, showing the response to a small [0.01*e* root-mean-square (rms)] sinusoidal signal at 1.1 MHz, is shown (Fig. 3B). The excellent S/N ratio of 42, obtained in an equivalent noise bandwidth of 23 Hz, corresponds to a charge sensitivity of $5.2 \times 10^{-5}\ e/\sqrt{\text{Hz}}$. Also shown (Fig. 3C) is the output spectrum for a signal at 137 MHz. At all frequencies, the gain showed a large modulation with dc gate charge, and went to zero when the reflected power was at an extremum, and the change in reflected power for a small additional charge was therefore small. This gain variation demonstrates that the observed signals are not contaminated by any appreciable capacitive cross-talk.

The very wide bandwidth of the RF-SET electrometer is illustrated in Fig. 4. The small-signal gain (obtained using an ~0.01*e* rms sine wave on the gate), varies less than 2 dB from 100 Hz to more than 40 MHz. Above 10 MHz, the filters (*26*) and heat sinking of the gate cable introduced some significant loss between the top of the cryostat and the device. A correction for this loss was applied after measuring the amplitude at the top of the cryostat for each frequency which gave one full period (1 electron) of the response, and this correction was consistent with the cable loss measured at room temperature. The loss in the gate line limited the range of frequencies investigated to <40 MHz, and causes the slightly larger estimated errors on the gain of ±1 dB above 5 MHz.

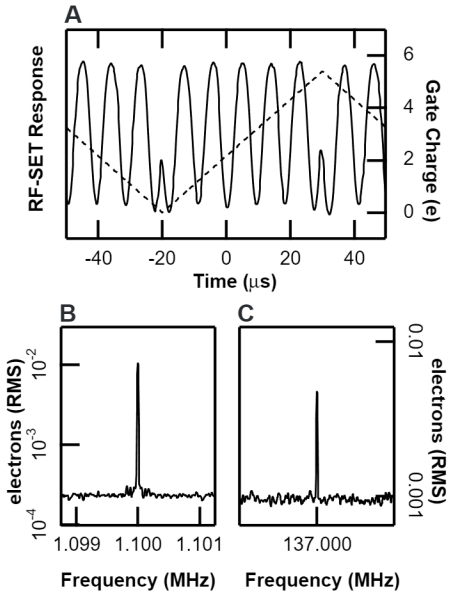

Fig. 3. High-frequency response of the RF-SET. (**A**) Time-domain response of RF-SET for a large (~5.5 electrons peak-to-peak) signal, 10 kHz triangle-wave (dotted line) applied to the gate. (**B**) Small-signal (0.01*e* rms) response for 1.1-MHz sine wave on gate. S/N is approximately 42, corresponding to a charge sensitivity of $5.2 \times 10^{-5}\ e/\sqrt{\text{Hz}}$. (**C**) Response to a small (0.006*e* rms) signal at 137 MHz.

The filters did allow a loss correction in a narrow range near 137 MHz. The gain obtained there (solid triangle) is not significantly lower, indicating that the 3-dB gain bandwidth of this RF-SET is probably in excess of 100 MHz.

Previous SET-based electrometers have suffered from large 1/*f* noise contributions at their operating frequencies (typically a few hundred hertz) which leads to much poorer sensitivities than the expected intrinsic limits (*27*). The charge sensitivity of the RF-SET system as a function of frequency was obtained by simultaneously measuring the system output noise and small signal gain, and is displayed (trace "N") in units of $e/\sqrt{\text{Hz}}$ on the right-hand axis of Fig. 4. Although the noise rises at lower frequencies, the sensitivity is $<10^{-4}\ e/\sqrt{\text{Hz}}$ for all frequencies above the 1/*f* corner at 3 kHz. This white noise floor is set by the noise of the 1.7 GHz amplifier in the present design, while the 1/*f* component is presumably due to background charge motion. This assignment of the noise sources is supported by the observation that the high-frequency system noise was independent of the gate charge and therefore SET gain, while the low-frequency noise was largest at gate charges corresponding to maxima of the gain, as expected for an input noise due to background charge motion.

Given the optimum carrier power and the observed depth of modulation (that is, the fractional change in reflected power), *D*, and knowing the noise temperature, $T_N = 10$ K, of the RF system, we can then calculate the expected sensitivity limit imposed by the RF amplifier. The device parameters and the predicted and measured

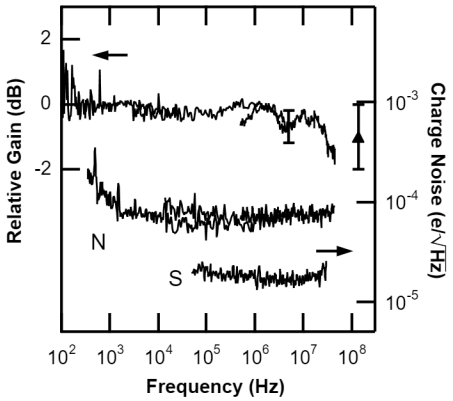

Fig. 4. Gain versus frequency for the RF-SET, showing the extremely large (~100 MHz) bandwidth of the device. Frequencies investigated were only limited by cable losses in the cryostat, and cause the somewhat larger error bars at the highest frequency (137 MHz, solid triangle) shown. Lower two traces show the system noise, expressed in $e/\sqrt{\text{Hz}}$, for operation in both normal (N) and superconducting (S) states.

sensitivities are detailed in Table 1. Not shown (*20*) are the results for a similar device that showed identical behavior in nearly every way, but with a larger noise contribution (about 1×10^{-4} $e/\sqrt{\text{Hz}}$) from the amplifier, due to a less efficient tuning circuit (larger value of C_{pad}) and therefore a smaller depth of modulation. The performance of both these tuning circuits and the observed white noise floors are in good agreement with the expected values. Finally, in Table 1, we include the predicted noise contribution of the amplifier for an optimized device. Tuning circuits with such high *Q*'s (that is, with low parasitic capacitance, C_{pad}) should be easily realizable, for example, by lithographically fabricating the tuning inductor on the SET chip.

Also shown (Fig. 4; trace "S") is the high-frequency noise obtained when the RF-SET is operated in its superconducting state, after removing the externally applied magnetic field. The optimum value of the carrier power in this superconducting state was about 6 dB higher, as would be expected because the onset of current then occurs at $4\Delta/e + e/2C_\Sigma \sim 1$ mV. In addition, the current near threshold and the dissipation in the RF-SET are more sharply peaked functions of the island charge, which increases the SET gain, and further reduces the amplifier's white noise contribution. We therefore observe an improved charge sensitivity in the superconducting state of 1.2×10^{-5} $e/\sqrt{\text{Hz}}$, which is approximately an order of magnitude better than typical, 1/*f*-noise-limited SET electrometers (*28*). The gain bandwidth in the superconducting case (*20*) was also greater than 50 MHz.

At present, we lack a theoretical model for the intrinsic noise of the RF-SET. We note, however, that the maximum instantaneous current (or voltage) in the device is comparable to that used in ordinary SETs. Because the intrinsic noise should be due to shot noise (*27*) of the tunnel junctions, we expect similar intrinsic noise for both the RF-SET and the ordinary SET. The high-frequency system noise varied by less than 3% with the dc gate charge, which supports the expectation that the intrinsic charge noise of the SET (*29*) is more than an order of magnitude below the presently achieved noise levels. By analogy with the practice used for very low-noise SQUIDs, we can equate our charge noise to an effective energy sensitivity of the RF-SET, $\delta E = (\delta q)^2/2C_\Sigma = 4.3 \times 10^{-33}$ J/Hz, or ~41 $\hbar$. For SQUIDs, the inclusion of quantum fluctuations (*30*) leads to a theoretical minimum of the energy sensitivity on the order of $\hbar$; some DC-SQUIDs have in fact attained (*31*) sensitivity on this order. For a device with optimized parameters (Table 1), the noise added due to the RF readout will be small enough for the RF-SET to approach this quantum limit.

The simultaneous achievement of high-sensitivity and large bandwidth should allow the RF-SET to perform time-domain counting of single electrons (compare with Fig. 3A) at very rapid rates. For example, in a detection bandwidth, *B*, the rms charge noise, ΔQ, is given by $\Delta Q = \delta q \times \sqrt{B}$, and is still much less than one electron, even using the entire available bandwidth of 100 MHz in the RF-SET (Table 2). Although conventional semiconductor transistors (FETs) can be very fast (speeds of gigahertz or more), they cannot attain single-electron resolution for bandwidths greater than a few kilohertz. If there were unity charge coupling to the RF-SET, however, the signal due to a single electron would still be 10 times greater than the standard deviation. Therefore, currents corresponding to several picoamperes can be measured with part-per-billion accuracy, by counting the individual electrons (*32*) which pass at an average frequency of $f = I/e$, or about 6 MHz/pA. Further improvements in the RF-SET performance could thus provide a means to realize capacitance or current standards (*6, 10*).

A drawback of all present SET devices is the rather low temperature required for operation, needed to ensure that thermal fluctuations are small compared to the charging energy, $kT \ll E_c = e^2/2C_\Sigma$. At the present device size (where $E_c \sim 2.1$ *K*), this is not too severe a restriction, because the performance of the RF-SET only degrades by about 3 dB at temperatures of 0.5 K. We note, however, that the RF-SET device concept can be applied to small capacitance double-junction devices achieved through any fabrication process. Therefore, advances in lithography may allow efficient operation of the RF-SET electrometer at even higher temperatures. Another interesting avenue is to use a higher gap superconductor, such as Nb (*33*). The larger threshold voltage allows the use of a larger carrier power, a lower noise contribution from the RF amplifier, and potentially even larger bandwidths. It should also be possible to combine the RF-SET with scanned-probe microscopy techniques, as in the recently demonstrated (*13*) single-electron transistor scanning electrometer (SETSE), which used an ordinary SET. This approach would add nanosecond temporal resolution and higher sensitivity to the spatially resolving capabilities of that microscope.

The main applications of the RF-SET electrometer will initially be in experiments on the physics of other single-electron and mesoscopic systems. SET electrometers have been used in this role, but because of their slow response, they have been limited to studying long-time or thermally averaged properties. The RF-SET can allow monitoring of individual tunneling or cotunneling (*34*) events and examination of the dynamics of these systems. One intriguing possibility with superconducting SET devices is the generation and manipulation of coherent superpositions of macroscopic quantum states. Such investigations first require a sensor (the RF-SET) that can measure the charge state of a macroscopic conductor with subelectron resolution, and on a timescale shorter than the decoherence time. This timescale is not yet known, but is probably (*36*) less than 100 μs. For technological applications, more work will be required in optimizing the coupling to the electrometer and in finding devices and detectors for which the RF-SET is best suited. We may hope, however, that as with SQUID amplifiers, there will be unanticipated and versatile uses for this device.

Table 1. RF-SET parameters and performance. Optimal is the predicted amplifier noise contribution for an optimized RF-SET, with the listed parameters. *D* is the depth of modulation of the reflected power. Measured charge noises were taken at 1.1 MHz in either the normal (δq_N) or superconducting (δq_S) state.

Parameter	Measured	Predicted	Optimal
R_{min} (kΩ)	195	–	50
C_Σ (aF)	450	–	250
C_{pad} (pF)	0.33	–	0.1
Q	6	6	21
D (%)	4	3.7	85
δq_N ($e/\sqrt{\text{Hz}}$)	4.7×10^{-5}	5×10^{-5}	6×10^{-6}
δq_S ($e/\sqrt{\text{Hz}}$)	1.2×10^{-5}	1×10^{-5}	1.75×10^{-6}
δ E ($\hbar$)	41 $\hbar$	27 $\hbar$	1.5 $\hbar$

Table 2. Comparison of electrometer sensitivities. For the FET, we assume an optimistic 1 nV/$\sqrt{\text{Hz}}$ and 1 pF input capacitance. The rms charge noise assumes a 100-MHz bandwidth.

Parameter	This experiment	Optimized RF-SET	Conventional FET
δq [$e/\sqrt{\text{Hz}}$]	1.2×10^{-5}	2×10^{-6}	$\sim 1 \times 10^{-2}$
ΔQ [*e*, rms]	0.1	0.02	100

REFERENCES AND NOTES

1. J. Clarke, *Proc. IEEE* **77**, 1208 (1989).
2. D. V. Averin and K. K. Likharev, *J. Low Temp. Phys.* **62**, 345 (1986).
3. T. A. Fulton and G. J. Dolan, *Phys. Rev. Lett.* **59**, 109 (1987).
4. K. K. Likharev, *IEEE Trans. Magn.* **MAG-23**, 1142 (1987).
5. G. Zimmerli, R. L. Kautz, J. M. Martinis, *Appl. Phys. Lett.* **61**, 237 (1992).
6. K. K. Likharev, in *Granular Electronics*, NATO ASI Series B: Physics, vol. 251, D. Ferry, Ed. (Plenum, New York, 1990).
7. A. N. Cleland, D. Esteve, C. Urbina, M. H. Devoret, *Appl. Phys. Lett.* **61**, 2820 (1992).

8. K. K. Likharev and A. B. Zorin, *J. Low Temp. Phys.* **59**, 347 (1985).
9. P. Lafarge *et al.*, *Z. Phys. B* **85**, 327 (1991).
10. M. W. Keller, J. M. Martinis, N. M. Zimmerman, A. H. Steinbach, *Appl. Phys. Lett.* **69**, 1804 (1996).
11. P. D. Dresselhaus, L. Ji, S. Han, J. E. Lukens, K. K. Likharev, *Phys. Rev. Lett.* **72**, 3226 (1994).
12. Y. Y. Wei, J. Weis, K. von Klitzing, K. Eberl, *Appl. Phys. Lett.* **71**, 2514 (1997).
13. M. J. Yoo *et al.*, *Science* **276**, 579 (1997).
14. For "standard" Al/AlO_x/Al junctions, the resistance is $R_J \sim 50$ kilohms and the capacitance $C_J \sim 0.2$ fF, so $1/2\pi R_J C_J \sim 16$ GHz. Alternatively, one can consider the rate at which electrons flow from drain to source in typical operation. This rate is just $f = I/e$, with I the current for which the modulation with gate is maximal, or approximately the threshold voltage over the minimum resistance of the SET, $I \sim e/C_\Sigma/4R_J$. Then this maximum tunneling rate is $f \sim 1/8R_J C_J$.
15. J. Petersson *et al.*, *Phys. Rev. B* **53**, 13272 (1996).
16. E. H. Visscher *et al.*, *Appl. Phys. Lett.* **68**, 2014 (1996).
17. B. Starmark, P. Delsing, D. B. Haviland, T. Claeson, in Extended Abstracts of the *6th International Superconductive Electronics Conference* (*ISEC '97*), H. Koch and S. Knappe, Eds. (PTB, Berlin, 1997), vol. 2, p. 391.
18. If the characteristic impedance of the coaxial cable, Z_0, is equal to the amplifier's impedance (50 ohms), then the effective impedance of the cable plus amplifier is purely real and equal to Z_0.
19. J. Niemeyer, *PTB-Mitt.* **84**, 251 (1974); G. J. Dolan, *Appl. Phys. Lett.* **31**, 337 (1977).
20. R. J. Schoelkopf *et al.*, data not shown.
21. The voltage reflection coefficient is given by $(Z - Z_0)/(Z + Z_0)$, and when $Z = R_T \gg Z_0$, then the total reflected power is proportional to $1 - 4Z_0/R_T$. The minimum resistance of the SET (Fig. 2A) is $R_{min} \sim 200$ kilohms, and the maximum is much larger. So without the resonant circuit (C_{pad} and L), the expected fractional change in reflection would be only one part in 10^3. The measured "depth of modulation" for this device was $D \sim 4\%$, in good agreement with the expected value $D = 4(Q^2)Z_0/R_{min} \sim 3.7\%$, given the value of the quality factor of the resonator, $Q = \omega_0 L/Z_0$ of ~6.
22. We estimate that the ac drain-source voltage swing across the SET is ~0.3 mV (or $V/Q \sim 50$ μV outside the resonator), based on the applied power of ~50 pW.
23. G. S. Krivoy and H. Koch, *J. Appl. Phys.* **74**, 2925 (1993); G. S. Krivoy and V. A. Komashko, *Physica B* **165/166**, 83 (1990).
24. P. Wahlgren and R. J. Schoelkopf, in preparation.
25. These sidebands have been observed directly, by examining the RF output in front of the rectifying diode on a gigahertz spectrum analyzer.
26. The gate and all dc leads had several low-pass "powder" filters of the type described in J. M. Martinis, M. H. Devoret, and J. Clarke [*Phys. Rev. B* **35**, 4682 (1987)].
27. A. N. Korotkov, *ibid.* **49**, 10381 (1994); A. N. Korotkov, D. V Averin, K. K. Likharev, S. A. Vasenko, in *Single-Electron Tunneling and Mesoscopic Devices*, H. Koch and H. Lübbig, Eds. (Springer-Verlag, Berlin, 1992), p. 45.
28. A charge noise of $9 \times 10^{-6}\ e/\sqrt{\text{Hz}}$ has recently been obtained with a transimpedance amplifier and a superconducting Al SET in a narrow band near 4 kHz (B. Starmark, private communication).
29. For dc drain-source biases much larger than the threshold voltage, a small but linearly increasing component of the high-frequency noise could be seen, which was consistent with the expected values of the output current noise of the SET, $S_I \sim eI$.
30. R. H. Koch, D. J. Van Harlingen, J. Clarke, *Appl. Phys. Lett.* **38**, 380 (1981).
31. D. J. Van Harlingen, R. H. Koch, J. Clarke, *ibid.* **41**, 197 (1982); M. W. Cromar and P. Carelli, *ibid.* **38**, 723 (1981).
32. This statement only applies to the noise introduced by the detector (RF-SET). A true calculation of the counting errors will depend also on the statistics of the electron transmission process itself.
33. Y. Harada, D. B. Haviland, P. Delsing, C. D. Chen, T. Claeson, *Appl. Phys. Lett.* **65**, 636 (1994).
34. D. V. Averin and Yu. V. Nazarov, *Phys. Rev. Lett.* **65**, 2446 (1990).
35. V. Bouchiat, thesis, University of Paris (1997).

36. We thank K. K. Likharev, J. M. Martinis, R. D. Grober, and J. Zmuidzinas for useful discussions, J. Webber and R. Bradley of the National Radio Astronomy Observatory for making the HEMT amplifier available, and B. Starmark for experimental assistance and for sharing prepublication results. The samples were fabricated at the Swedish Nanometer Laboratory. Supported by NSF grants DMR-9216121 and DMR-9701427, and by ESPRIT (CHARGE 22953). P.W. wishes to acknowledge generous support from the Wallenberg Foundation.

29 December 1997; accepted 30 March 1998

Salts on Europa's Surface Detected by Galileo's Near Infrared Mapping Spectrometer

T. B. McCord, G. B. Hansen, F. P. Fanale, R. W. Carlson, D. L. Matson, T. V. Johnson, W. D. Smythe, J. K. Crowley, P. D. Martin, A. Ocampo, C. A. Hibbitts, J. C. Granahan, the NIMS Team

Reflectance spectra in the 1- to 2.5-micrometer wavelength region of the surface of Europa obtained by Galileo's Near Infrared Mapping Spectrometer exhibit distorted water absorption bands that indicate the presence of hydrated minerals. The laboratory spectra of hydrated salt minerals such as magnesium sulfates and sodium carbonates and mixtures of these minerals provide a close match to the Europa spectra. The distorted bands are only observed in the optically darker areas of Europa, including the lineaments, and may represent evaporite deposits formed by water, rich in dissolved salts, reaching the surface from a water-rich layer underlying an ice crust.

Europa is the second Galilean satellite outward from Jupiter. It is a lunar-sized object with a water-ice surface of relatively young geologic age (*1*, *2*). Its density and gravity field suggest a differentiated object with an Fe-rich core and silicate mantle underlying an ice-rich crust (*3*). The surface features and young age (*4*) suggest recent resurfacing, perhaps from a liquid water ocean existing between a relatively thin ice crust and the silicate mantle. Tidal heating has been suggested as the energy source to maintain an ocean in this relatively cold part of the solar system (surface temperatures on Europa range from 100 to 120 K) (*5*). The existence of heat and water plus organic molecules (*6*) has led many to speculate whether Europa's ocean might be an environment with the potential for sustaining life (*7*).

Ground-based telescope observations show that Europa exhibits a high visual albedo and other spectral reflectance characteristics in the 1- to 5-μm wavelength range that were reported to indicate the dominance (>85% by weight) of surface water ice or frost (or both) and only a few weight percent impurities, with the possible presence of iron-bearing minerals that reduce the visible brightness in some regions (*2*, *8*). In addition, forms of sulfur-rich species, including sulfur allotropes, SO, SO_2, and H_2S, have been suggested as impurities in Europa's surface on the basis of ultraviolet and visible spectroscopy and Voyager multispectral images (*9*, *10*). These sulfur-rich species are thought to be derived from materials sputtered from Io and carried to Europa by Jupiter's magnetosphere, although an interior origin has also been suggested (*10*).

Early observations by the Near Infrared Mapping Spectrometer (NIMS) (*11*) indicated a surface of almost pure water ice for a north polar region of Europa (*12*), consistent with the earlier interpretations of the telescopic spectra. Here, we discuss subsequent NIMS observations of Europa that indicate the presence of hydrated minerals. Water-related spectral features dominate the NIMS reflectance spectra in the 1- to 3-μm range for Europa (Fig. 1). These features are due to vibration modes and combinations of these modes for H–O–H (*13*) in ice or in association with hydrated species (*14*, *15*). The features include absorption bands centered near 1.04, 1.25, 1.5, and 2 μm; a weak temperature-sensitive ice band at 1.65 μm on the edge of the 1.5-μm feature (*16*); and the fundamental O–H stretching transition near 3 μm. Water is strongly absorbing longward of 2.5 μm and is mostly responsible for the low reflectance in this region for all icy Galilean satellites (*6*).

T. B. McCord, G. B. Hansen, F. P. Fanale, P. D. Martin, C. A. Hibbitts, Hawaii Institute of Geophysics and Planetology, University of Hawaii, Honolulu, HI 96822, USA. R. W. Carlson, D. L. Matson, T. V. Johnson, W. D. Smythe, A. Ocampo, Jet Propulsion Laboratory, Pasadena, CA 91109, USA.
J. K. Crowley, U.S. Geological Survey, MS954, Reston, VA 20192, USA.
J. C. Granahan, STI Inc., Honolulu, HI 96813, USA.